frontiers in Plant Science

TYPE Original Research
PUBLISHED 05 November 2026
DOI 10.3389/fpls.2026.1979213

Check for updates

OPEN ACCESS

EDITED BY
Guillaume Pilot,
Virginia Tech, United States

REVIEWED BY
Zhi-Ming Yu,
Hangzhou Normal University, China
NAVEEN SHARMA,
Michigan State University, United States
Jorge El-Azaz,
University of Wisconsin-Madison, United States

*CORRESPONDENCE
Hui Zhang
huiz2006@163.com

RECEIVED 26 August 2026
REVISED 09 October 2026
ACCEPTED 13 October 2026
PUBLISHED 05 November 2026

CITATION
Zhai N, Zhang P, Liu Y, Zhou H, Xu G, Li Z, Liu P, Jin L, Zheng Q and Zhang H (2026) Silencing of *NtIPMDs* is associated with impaired chloroplast development and altered amino acid metabolism in tobacco.
Front. Plant Sci. 17:1979213.
doi: 10.3389/fpls.2026.1979213

COPYRIGHT
© 2026 Zhai, Zhang, Liu, Zhou, Xu, Li, Liu, Jin, Zheng and Zhang. This is an open-access article distributed under the terms of the Creative Commons Attribution License (CC BY). The use, distribution or reproduction in other forums is permitted, provided the original author(s) and the copyright owner(s) are credited and that the original publication in this journal is cited, in accordance with accepted academic practice. No use, distribution or reproduction is permitted which does not comply with these terms.

Silencing of *NtIPMDs* is associated with impaired chloroplast development and altered amino acid metabolism in tobacco

Niu Zhai, Peipei Zhang, Yali Liu, Huina Zhou, Guoyun Xu, Zefeng Li, Pingping Liu, Lifeng Jin, Qingxia Zheng and Hui Zhang*

China Tobacco Gene Research Center, Zhengzhou Tobacco Research Institute of CNTC, Zhengzhou, China

Isopropylmalate dehydrogenase (IPMD) catalyzes the oxidation and decarboxylation of 3-isopropyl-L-malate (IPM) to form 4-methyl-2-oxovalerate in leucine biosynthesis. Although *IPMD* genes are well studied in Arabidopsis, their functions in other plants remain unclear. Here, we investigated two chloroplast-localized IPMDs (NtIPMD1 and NtIPMD2) in tobacco. RNAi-mediated silencing of both genes caused variegated leaves, stunted growth, reduced chlorophyll content, and abnormal chloroplast ultrastructure. Transcriptome analysis showed down-regulation of photosynthesis-related genes, consistent with impaired photosynthetic capacity. Metabolomic profiling revealed that most amino acids, particularly valine, accumulated in *NtIPMD*-RNAi lines, whereas leucine increased only slightly. Phytohormone analysis further showed reduced ABA and GA levels. These results indicate that *NtIPMDs* silencing is associated with impaired chloroplast development and altered amino acid metabolism. The strong valine accumulation and slight leucine change suggest that leucine content may not directly reflect IPMD activity, and these effects may be indirect consequences of metabolic pathway. Further studies are needed to clarify whether NtIPMD has functions beyond leucine biosynthesis.

KEYWORDS
amino acid, chloroplast, development, *Nicotiana tabacum*, *NtIPMD*

Introduction

Chloroplasts are unique organelles in plants and algae that mediate numerous biological processes. Beyond their fundamental role in photosynthesis, chloroplasts are essential for the synthesis of amino acids, fatty acids, lipids, phytohormones, and other critical metabolites (Waters and Langdale, 2009; Li et al., 2022; Rui et al., 2025; Scotti and Tamburino, 2026). Chloroplast-localized proteins are encoded by both the chloroplast and nuclear genomes. The expression of these genes is vital for both the development and functional maintenance of the organelle. These genes are transcribed by two types of polymerases: one encoded in the chloroplast (PEP) and the other encoded in the nucleus (NEP). Each polymerase has its own

specific tasks in managing gene expression (Hess and Borner, 1999). The maturation of chloroplasts is closely linked to enhanced plant biomass accumulation. This developmental process is complex and tightly regulated, involving numerous genes that facilitate dynamic signaling between plastids and the nucleus (Liebers et al., 2022; Zhang et al., 2023). Such genes are recognized as key regulators governing various stages of chloroplast development (Zheng et al., 2016). Mutations in these genes can disrupt chloroplast biogenesis, affecting chloroplast morphology, number, and size, which in turn influence leaf coloration, shape, and photosynthetic efficiency (Chang et al., 2021). For instance, the Arabidopsis *var2* mutant, which lacks the VAR2/AtFtsH2 subunit of the FtsH protease complex, displays pronounced leaf variegation. This complex is involved in the biogenesis and repair of photosystem II, highlighting how genetic mutations can impact chloroplast structure and function (Liu et al., 2010; Wang et al., 2022).

Leucine, a branched-chain amino acid (BCAA), is an essential amino acid for mammals because they cannot synthesize it *de novo*. It plays key roles in protein synthesis, immune function, and nutritional metabolism (Siddik and Shin, 2019). In contrast to other amino acids, *de novo* leucine synthesis occurs exclusively in plants and microorganisms. The pathway initiates with α-ketoisovalerate, the keto acid corresponding to valine, which is successively converted through three enzymatic steps into the leucine precursor α-ketoisocaproate via transamination (Binder, 2010). This biosynthesis is regulated by three rate-limiting enzymes: isopropylmalate synthase (IPMS), isopropylmalate isomerase (IPMI), and isopropylmalate dehydrogenase (IPMD). IPMD catalyzes the oxidation and decarboxylation of 3-isopropyl-L-malate (IPM) to form 4-methyl-2-oxovalerate. IPMD has been extensively studied in microbial systems for decades, with work focused on its catalytic mechanisms, substrate recognition, and crystal structures (Fujita et al., 2001; Pallo et al., 2014; Graczer et al., 2016; Miggiano et al., 2020). In contrast, its functions in plants remain poorly characterized. The *IPMD* genes have been isolated and cloned from several plant species, including rapeseed, potato, and Arabidopsis (Ellerstrom et al., 1992; Jackson et al., 1993; Nozawa et al., 2005). In Arabidopsis, three *IPMD* genes have been identified. *AtIPMD1* is involved in both glucosinolate and leucine biosynthesis (He et al., 2009), whereas *AtIPMD2* and *AtIPMD3* participate specifically in leucine metabolism and are critical for pollen and embryo development (He et al., 2011a). Interestingly, single knockout of these genes did not result in visible phenotypic alterations. Structural and enzymatic studies have identified key amino acid residues that determine the functional divergence between the leucine and aliphatic glucosinolate biosynthetic pathways (He et al., 2011b; Lee et al., 2016). Recent studies have shown that AtIPMD forms a protein complex with AtIPMI. This complex functions in methionine chain elongation, a step in the biosynthesis of glucosinolates, and leucine biosynthesis, suggesting a coordinated regulation of these two pathways (Chen et al., 2021). Moreover, IPMD has been implicated in acylsugar synthesis in species such as *Solanum pennellii* and *Nicotiana benthamiana* (Slocombe et al., 2008). Despite its widespread presence in plants, the functions of *NtIPMD* genes, particularly their roles in growth and development, remain largely unexplored in many species.

In this study, we characterized two chloroplast-localized isopropylmalate dehydrogenases in tobacco, designated NtIPMD1 and NtIPMD2. Given the extremely high sequence identity between the two genes, we used an RNAi construct targeting a conserved region to silence both genes simultaneously. RNAi-mediated suppression of *NtIPMDs* resulted in degreening and growth retardation. Further observations indicated a reduction in chloroplast number and abnormal thylakoid structure with fewer lamellae, suggesting that *NtIPMDs* are involved in chloroplast development. Together, our results indicate that NtIPMDs are associated with chloroplast development and plant growth in tobacco, and provide a basis for further studies on the functional diversity of plant IPMDs.

Materials and methods

Plant materials and growth conditions

The tobacco cultivar K326 (*Nicotiana tabacum* L.), maintained in our laboratory, was used for transgenic experiments and gene expression analysis. Seeds were sown and grown in plastic pots under standard conditions (16 h light at 28 °C/8 h darkness at 23 °C). Tissues for qPCR experiments were collected from plants at the vigorous growth stage.

Phylogenetic analysis

IPMD protein sequences from tobacco and other plant species were aligned using Muscle implemented in MEGA 7.0. An unrooted neighbor-joining (NJ) tree was constructed with the *p*-distance model and 1,000 bootstrap replicates. Bootstrap values >50% are shown at the nodes. The tree was visualized and edited using TVBOT (Xie et al., 2023).

Vector construction and tobacco transformation

The RNAi vector was constructed as previously described (Chuang and Meyerowitz, 2000). The conserved coding sequence (CDS) fragment of *NtIPMDs* was amplified and cloned into the pBWA(V) HS vector via homologous recombination using an In-Fusion HD Cloning Kit (Clontech, Japan). The construct was introduced into tobacco (K326) using *Agrobacterium tumefaciens* (strain GV3101)-mediated transformation, following established protocols (Svab and Maliga, 1993).

Total RNA isolation and qRT-PCR

For *NtIPMD*-RNAi plants, the leaves displaying the most severe phenotype were sampled. Tissues were immediately frozen in liquid nitrogen and ground to a fine powder for RNA extraction. RNA isolation, cDNA synthesis, and qRT-PCR were performed as described previously (Zhang et al., 2022). Total RNA was extracted using the Polysaccaride/polyphenol Plant Total RNA Mini Kit (R318-50, GeneBetter life science, Beijing). First-strand cDNA

was synthesized with the Transcriptor First Strand cDNA Synthesis Kit (Roche). qRT-PCR was performed on a LightCycler96 (Roche, Switzerland) using 10 µl of 2× SYBR Green premix (Roche) per reaction. The thermal profile was 95 °C for 10 min, followed by 40 cycles of 95 °C for 10 s, 60 °C for 20 s, and 72 °C for 20 s. The tobacco *Nt26S* (Li et al., 2023) and *NtL25* (Baek et al., 2017) genes were used as the internal reference controls. Three biological replicates and three technical replicates were analyzed for each sample. All gene-specific primers used for qRT-PCR are listed in Supplementary Table S1.

Subcellular localization

To investigate the subcellular localization of NtIPMDs, we generated constructs in which *NtIPMD1* and *NtIPMD2* were fused to GFP at their C-termini under the control of the 35S promoter (35S::*NtIPMD1*-GFP and 35S::*NtIPMD2*-GFP). The coding regions of *NtIPMD1* and *NtIPMD2* (excluding the stop codon) were amplified from K326 cDNA. The resulting construct was introduced into *A. tumefaciens* strain GV3101 and transiently expressed in *Nicotiana benthamiana* leaves via agroinfiltration. GFP fluorescence was examined 24 hours post-infiltration using a TCS STED CW confocal laser microscope (LEICA, Wetzlar, Germany). The primers used here are listed in Supplementary Table S2.

Measurement of chlorophyll content

Chlorophyll content was determined using a plant chlorophyll assay kit (JLCS1422, Jingkang Bioengineering Co. LTD, Shanghai) with a spectrophotometric method, measuring absorbance at 645 nm and 663 nm for chlorophyll a and chlorophyll b, respectively. Chlorophyll content was quantified in leaves of K326 and *NtIPMD*-RNAi lines at the seedling stage.

Microscopic analysis

For light microscopy, paraffin sections were prepared from fully expanded leaves of WT and *NtIPMD*-RNAi plants. Leaf tissues were fixed in FAA solution and vacuum-infiltrated for 30 min. Dehydration was carried out using a series of ethanol solutions (50-100%), followed by treatment with a xylene gradient (25-100%). Samples were soaked in paraffin at 60 °C for 3 days and then embedded in paraffin blocks. Sections of about 8 µm were cut using a microtome, dewaxed, and stained with safranin and Fast Green FCF before observation with a light microscope.

For TEM (transmission electron microscopy) analysis, Sample preparation was performed as previously reported (Kowalewska et al., 2016). Fresh leaf pieces were fixed in 2.5% glutaraldehyde in phosphate buffer. Centrifugation was used to ensure the samples were fully immersed in buffer. After fixation, samples were treated with 1% osmium tetroxide, followed by staining with uranyl acetate. Dehydration was carried out using an ethanol series before embedding in Spurr's resin and sectioning into ultrathin slices. The sections were examined with a Hitachi HT7800 TEM (Tokyo, Japan).

RNA-seq and data analysis

Total RNA was isolated from tobacco leaves with TRIzol reagent (Invitrogen). The integrity and concentration of RNA were assessed with a NanoDrop 2000 spectrophotometer. Sequencing libraries were prepared from qualified RNA and sequenced on an Illumina HiSeq platform at Novogene (Beijing, China). Data analysis was conducted as follows: raw reads were evaluated by FastQC (https://www.bioinformatics.babraham.ac.uk/projects/fastqc/) (Brown et al., 2017); high quality reads (Q > 20) were obtained using NGSTools (Fumagalli et al., 2014); clean reads were aligned to the K326 reference genome (https://solgenomics.net/organism/Nicotiana_tabacum/genome) (Edwards et al., 2017) with HISAT2 (Kim et al., 2019); gene expression levels were estimated with Cufflinks (Ghosh and Chan, 2016); differentially expressed genes (DEGs) were identified with DESeq2 (Love et al., 2014) ($|\log_2 FC| > 1$ and q-value < 0.05); Gene Ontology (GO) and Kyoto Encyclopedia of Genes and Genomes (KEGG) enrichment analyses were carried out with clusterProfiler (Yu et al., 2012).

Measurement of amino acid content

Amino acid quantification was performed on an AB Sciex QTRAP 6500 LC-MS/MS system. Samples were extracted with 70% methanol/water, centrifuged, and the supernatant was analyzed on an ACQUITY BEH Amide column (100 mm × 2.1mm i.d., 1.7 µm) at 40 °C with a 2 µL injection volume. Separation used a gradient of 2 mM ammonium acetate in water (A) and acetonitrile (B), both with 0.04% formic acid. The gradient was initiated at 90% B for 1.2 min, then decreased to 60% B at 9 min and 40% B at 11 min, and returned to 90% B at 15 min, with a flow rate of 0.4 mL/min. Mass spectrometric data were acquired in both positive and negative ion modes, with the source temperature set at 550 °C, ion spray voltage at 5500 V (positive) and -4500 V (negative), and curtain gas at 35.0 psi. Declustering potential (DP) and collision energy (CE) were optimized for multiple reaction monitoring (MRM) transitions of individual amino acids. Peaks were identified by comparing retention times and MRM transitions with those of reference standards, and quantified using external calibration curves.

Measurement of phytohormone content

Phytohormone profiling was performed on a UPLC-ESI-MS/MS system consisting of an ExionLC AD UPLC and a QTRAP 6500+ mass spectrometer (SCIEX). Frozen leaf samples (50 mg) were ground in liquid nitrogen and extracted with 1 mL methanol/water/formic acid (15:4:1, v/v/v) containing 10 µL of internal standard mixture (100 ng/mL). After vortexing for 10 min and centrifugation at 12,000 rpm for 5 min at 4 °C, the supernatant was evaporated to dryness, reconstituted in 100 µL of 80% methanol, and filtered through a 0.22 µm membrane. Separation was achieved on a Waters ACQUITY UPLC HSS T3 C18 column (100 mm × 2.1 mm i.d., 1.8 µm) at 40 °C with a 2 µL injection volume. The mobile phases were water (A) and acetonitrile (B), both containing

0.04% acetic acid. The gradient was 5% B at 0–1 min, increased to 95% B at 1–8 min, held at 95% B for 8–9 min, and returned to 5% B at 9.1–12 min, at a flow rate of 0.35 mL/min. MS data were acquired in both positive and negative ion modes with scheduled MRM, source temperature 550 °C, ion spray voltage 5500 V (positive) and -4500 V (negative), and curtain gas 35 psi. DP and CE were optimized for each MRM transition. Peaks were identified by comparing retention times and MRM transitions with reference standards, and quantified using internal standard calibration curves.

Results

Characterization of *NtIPMD* genes

A comprehensive genomic survey of the tobacco (*Nicotiana tabacum* L.) genome (Wang et al., 2024) revealed two putative genes encoding isopropylmalate dehydrogenase, which were designated *NtIPMD1* and *NtIPMD2*. Sequence alignment revealed that the two paralogs share 97.28% amino acid sequence identity, suggesting a recent gene duplication event. Meanwhile, the NtIPMD proteins exhibit an approximately 79.5% amino acid identity with the three AtIPMD proteins from *Arabidopsis thaliana* (Supplementary Figure S1). Phylogenetic analysis showed that IPMD proteins from the same plant species or closely related species clustered together, with the two NtIPMDs from tobacco forming a tight group that reflects their high sequence identity (Figure 1A). RNA-seq data showed that the two *NtIPMDs* expressed in all tissues examined, including roots, stems, and leaves at the seedling (S), vigorous growth (V), and mature (M) stages, as well as in flowers and capsules (Figure 1B). qRT-PCR analysis revealed that the *NtIPMDs* expressed mainly in leaves at the vigorous growth stage (Figure 1C). To investigate the subcellular localizations, 35S::*NtIPMDs*-GFP fusion vectors were generated and expressed it in *N. benthamiana*. As shown in Figure 1D, both the two NtIPMDs localized to chloroplasts.

NtIPMDs influence chlorophyll biosynthesis in tobacco leaves

To elucidate the function of *NtIPMD* genes in tobacco, we employed an RNA interference (RNAi) approach to investigate their roles in plant growth and development. Given the extremely high sequence identity between the two *NtIPMD* genes, we were unable to silence each gene individually. Consequently, we generated an RNAi construct targeting a conserved region to suppress both genes at the same time. Three independent transgenic lines (R1, R2, and R3) were obtained and designated *NtIPMD*-RNAi lines (hereafter referred to as knockdown lines). All three lines exhibited leaf variegation and reduced growth rate (Figures 2A, B). qRT-PCR confirmed significantly reduced *NtIPMDs* expression in all three lines compared to the wild type (Figure 2C). Chlorophyll content was significantly decreased in all three lines, including chlorophyll a and chlorophyll b (Figures 2D, E). Although the *NtIPMD*-RNAi plants eventually grew and flowered after an extended period, most leaves displayed a variegated phenotype at the vigorous growth stage (Figure 2F). For subsequent detailed analyses, R1 was used as a representative line.

NtIPMDs affect chloroplast development of tobacco leaves

To evaluate the impact of *NtIPMDs* on chloroplast development, we examined leaf cross-sections under light microscopy. The *NtIPMD*-RNAi plants showed a marked reduction in chloroplast number and disorganized palisade cell arrangement (Figure 3A). We further analyzed the chloroplast ultrastructure in both K326 and *NtIPMD*-RNAi plants using transmission electron microscopy (Figure 3B). Chloroplasts in K326 displayed typical morphology with densely stacked grana lamellae. In contrast, the few chloroplasts observed in mesophyll cells of *NtIPMD*-RNAi plants exhibited abnormal thylakoid architecture and a reduced number of lamellae (Figures 3C–E), indicating that *NtIPMDs* silencing impairs chloroplast morphology.

To investigate the role of NtIPMDs in chloroplast function and plant growth, we measured key photosynthetic parameters. *NtIPMD*-RNAi plants showed significant reductions in the maximum quantum efficiency of PSII (Fv/Fm) and the electron transport rate (ESRII) compared to the K326 (Figures 4A, B). Additionally, qRT-PCR analysis revealed consistent down-regulation of genes associated with PSI/PSII, chlorophyll biosynthesis, light-harvesting complexes (LHCs), and tetrapyrrole metabolism in the *NtIPMD*-RNAi plants (Figures 4C–F). These findings suggest that *NtIPMDs* are involved in chloroplast development and function.

Transcriptome analysis of *NtIPMD*-RNAi lines and K326 leaves

RNA-seq analysis was performed on rosette stage leaves from K326 and *NtIPMD*-RNAi lines. Among the 47,932 genes detected, 9,572 were differentially expressed relative to K326, with 4,668 up-regulated and 4,904 down-regulated. GO enrichment analysis revealed that these differentially expressed genes (DEGs) were primarily related to photosynthesis under biological process (BP); photosystem I, photosystem II and the chloroplast thylakoid membrane under cellular component (CC); and ATP binding and chlorophyll binding under molecular function (MF) (Figure 5A). KEGG pathway analysis further indicated significant enrichment of DEGs in photosynthesis, porphyrin and chlorophyl metabolism, carbon fixation in photosynthetic organisms, plant hormone signal transduction and several amino acid metabolism pathways (Figure 5B). In contrast, GO analysis did not identify strongly enriched amino acid-related terms.

Given the role of NtIPMDs in chloroplast development, we specifically examined expression changes in genes encoding chlorophyll A/B binding proteins (Figure 5C), chlorophyll synthesis/development (Figure 5D), and PSI/PSII components (Figure 5E). RNA-seq data showed that these genes were down-regulated by 1.4-4.4-fold ($\log_2$FC) in *NtIPMD*-RNAi plants relative to K326. These results imply that *NtIPMDs* affect the expression of photosynthesis-related genes, thereby consistent with reduced photosynthetic capacity of tobacco leaves.

10.3389/fpls.2026.1979213

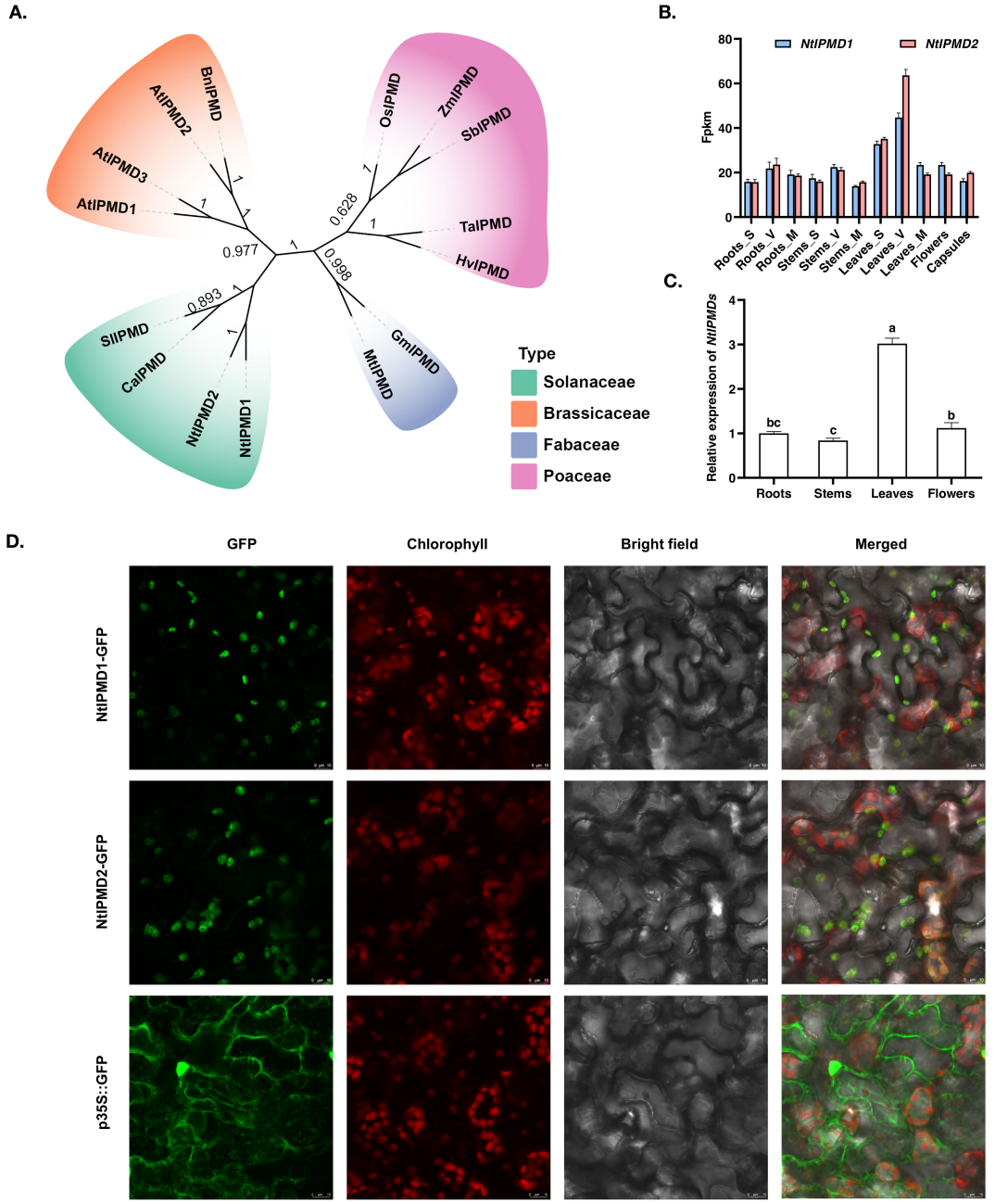


FIGURE 1
Phylogenetic analysis and subcellular location of *NtIPMDs* in tobacco. **(A)** Phylogenetic tree of IPMD proteins in tobacco and other plants. The unrooted neighbor-joining tree was constructed using MEGA with the p-distance model and 1,000 bootstrap replicates. Bootstrap values (>50%) are shown at the nodes. At, *Arabidopsis thaliana*; Bn, *Brassica napus*; Sl, *Solanum lycopersicum*; Ca, *Capsicum annuum*; Nt, *Nicotiana tabacum*; Mt, *Medicago truncatula*; Gm, *Glycine max*; Hv, *Hordeum vulgare*; Ta, *Triticum aestivum*; Sb, *Sorghum bicolor*; Zm, *Zea mays*; Os, *Oryza sativa*. **(B)** Expression levels of *NtIPMDs* in different tissues at the seedling (S), vigorous growth (V), and mature (M) stages based on transcriptome data. (The raw data sets analyzed are available on NCBI under accession: PRJNA1404846). **(C)** Expression levels of *NtIPMDs* in different tissues at the vigorous growth stage by qRT-PCR. The expression in roots was defined as "1". Different letters indicate significant differencess determined by one-way ANOVA (Tukey's multiple comparisons test, $p < 0.05$). **(D)** Subcellular location of NtIPMDs-GFP in tobacco cells.

NtIPMDs affect amino acid and phytohormone metabolism

To evaluate the influence of *NtIPMDs* on amino acid biosynthesis, we quantified 20 amino acids in K326 and *NtIPMD*-RNAi plants using LC-MS. The results showed that nearly all detectable amino acids accumulated to markedly higher levels in the *NtIPMD*-RNAi plants than in the wild type (Figure 6). Notably, valine (Val) content increased by approximately16.6-fold. Leucine (Leu) levels also increased modestly, suggesting that *NtIPMDs* are unlikely to play a direct role in leucine biosynthesis.

Abscisic acid (ABA) and gibberellin (GA) are well-established regulators of chloroplast development and photosynthetic efficiency (Cackett et al., 2022; Altamura et al., 2024). Given that the *NtIPMD*-RNAi lines showed severe chloroplast defects, we measured the levels of these hormones to examine whether hormonal changes

10.3389/fpls.2026.1979213

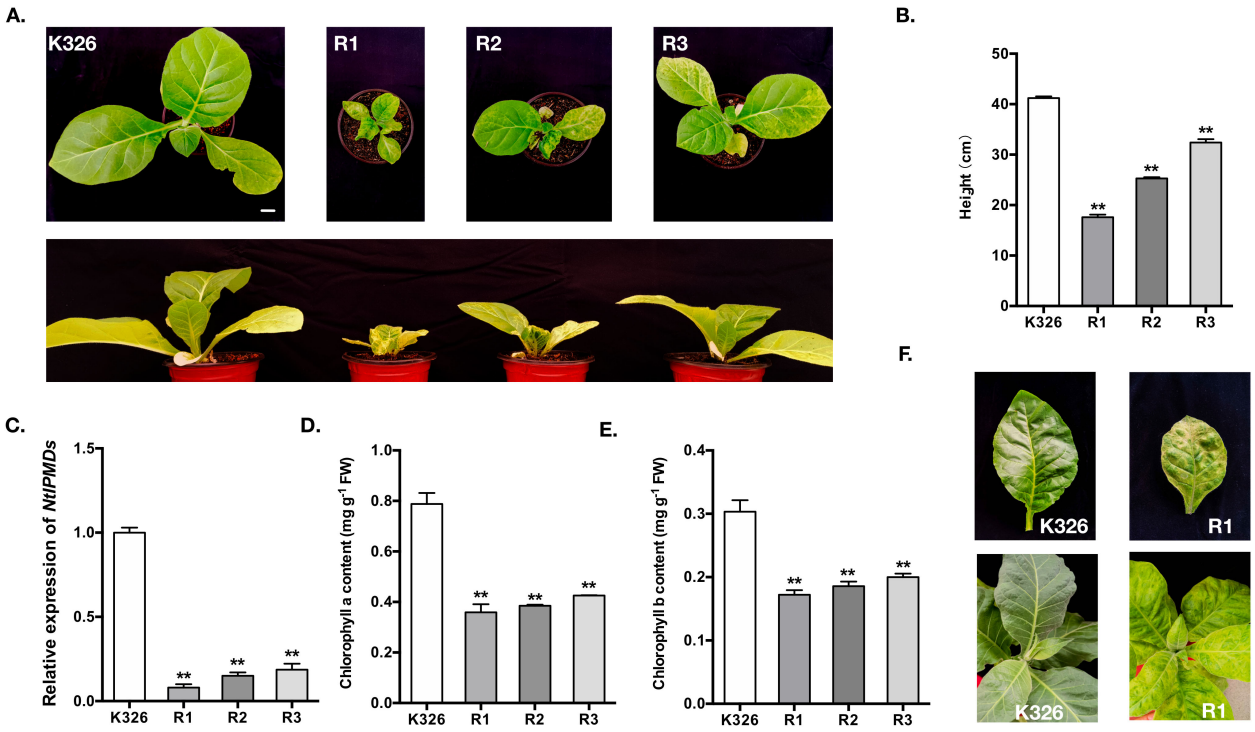


FIGURE 2
Phenotypic analysis of the *NtIPMD*-RNAi plants compared with wild-type K326. **(A)** Top and side view of seedlings of *NtIPMD*-RNAi and wild-type plants. **(B)** Plant height of *NtIPMD*-RNAi and wild-type plants. **(C)** Relative expression of *NtIPMDs* in leaves. **(D, E)** Chlorophyll a and chlorophyll b content analysis of *NtIPMD*-RNAi and wild-type plants. **(F)** Phenotypes of *NtIPMD*-RNAi (R1) and wild-type plants at the vigorous growth period. Data are presented as mean ± SD, $^{**}p < 0.01$.

accompany these phenotypes. Compared with K326, *NtIPMD*-RNAi plants exhibited approximately 60% and 50% reductions in ABA and GA contents, respectively (Figure 7A). Consistently, the expression of key biosynthesis genes, 9-cis-epoxycarotenoid dioxygenase (*NtNCED*) and gibberellin 20 oxidase 1-like (*NtGA20ox1*), was decreased by 76% and 87%, respectively (Figure 7B).

Discussion

In Arabidopsis, the three *IPMD* genes serve distinct roles: *AtIPMD1*is primarily involved in methionine chain elongation, whereas *AtIPMD2* and *AtIPMD3* function redundantly in leucine biosynthesis (He et al., 2010, 2011). These genes exhibit gene dosage-dependent effects, as evidenced by the lethality of *ipmdh2 ipmdh3* double mutant and the severe chlorophyll deficiency and reduced fresh weight observed in *ipmdh1 / ipmdh1 IPMDH2 / ipmdh2 ipmdh3 / ipmdh3* plants (He et al., 2011a). In allotetraploid tobacco, we identified two recently duplicated paralogs NtIPMD1 and NtIPMD2 with 97.28% amino acid identity. Phylogenetic analysis revealed only ~ 79.5% sequence similarity between tobacco and Arabidopsis IPMDs, pointing to potential functional divergence. Virus-induced gene silencing (VIGS)-silenced plants targeting a conserved region shared by *NtIPMD1* and *NtIPMD2* exhibited a variegated phenotype (Supplementary Figure S3). In addition, we were unable to obtain CRISPR-knockout plants, suggesting that complete loss of *NtIPMDs* function may be lethal in tobacco. We therefore used RNAi targeting their conserved region to lower the expression of both genes for phenotype observation. Unlike Arabidopsis, where single-gene *IPMD* mutants can grow, tobacco needs functional *NtIPMDs* for normal vegetative growth.

Our results show that NtIPMDs localize to chloroplasts and their silencing is associated with impaired chloroplast development in tobacco. The *NtIPMD*-RNAi lines exhibited leaf variegation, reduced growth, lower chlorophyll content, and abnormal chloroplast ultrastructure. together with reduced Fv/Fm and ETRII and downregulation of photosynthesis-related genes (Figures 2–4). Given that *NtIPMDs* function in an essential metabolic pathway, these chloroplast defects may be indirect consequences of metabolic disruption rather than direct regulation by *NtIPMDs*. Whether *NtIPMDs* directly regulate choroplast development or these defects result from metabolic disruption remains to be determined. Similar observations have been reported for other chloroplast-localized metabolic enzymes, such as NtIPDS (Zhang et al., 2024).

Although NtIPMDs share high sequence similarity with Arabidopsis AtIPMD2, which is directly involved in leucine biosynthesis (He et al., 2011a), our metabolic profiling showed higher rather than lower levels of leucine and a strong accumulation of valine in *NtIPMD*-RNAi plants (Figure 6). This result was unexpected. However, free amino acid levels do not directly reflect metabolic flux through biosynthetic pathways (Dellero et al., 2020). In plants with severe growth defects caused by gene silencing or metabolic mutations, the balance between protein synthesis and degradation is often disrupted, leading to the accumulation of free amino acids (Ali et al., 2015; Gouveia et al., 2026). Similar to

10.3389/fpls.2026.1979213

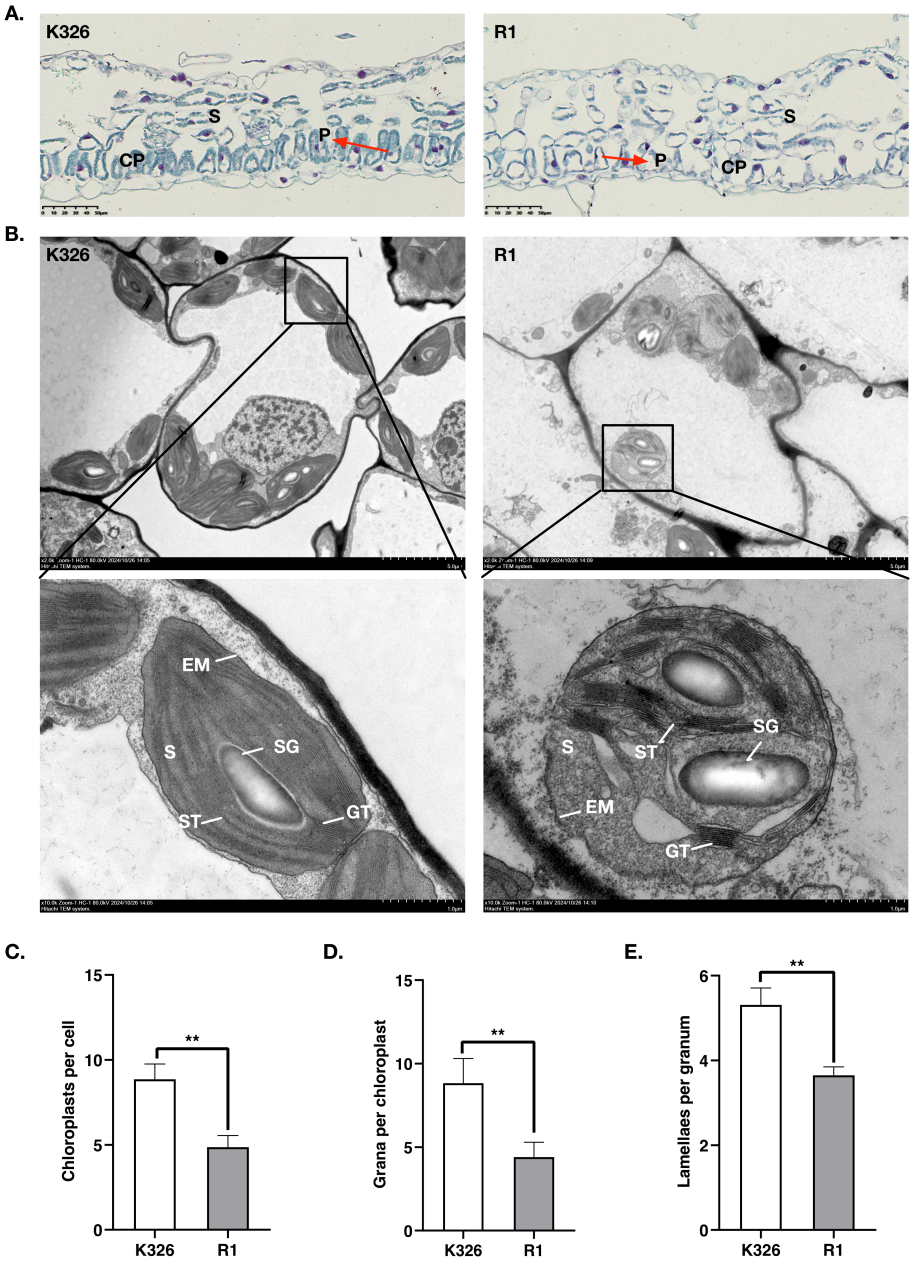


FIGURE 3
Histology observation of tobacco leaves of K326 and *NtIPMD*-RNAi plants. **(A)** Paraffin sections of K326 and R1. CP, chloroplast; S, spongy mesophyll; P, palisade mesophyll. **(B)** Transmission electron micrographs of K326 and R1. EM, envelope membranes; S, stroma; SG, starch granule; ST, stroma thylakoids; GT, grana thylakoids. **(C)** Quantification of chloroplasts per mesophyll cell. Data are presented as mean ± SD (n = 10 cells per genotype), $^{**}p < 0.01$. **(D)** Quantification of grana per chloroplast. Data are presented as mean ± SD (n = 6 chloroplasts per genotype), $^{**}p < 0.01$. **(E)** Quantification of lamellae per granum. Data are presented as mean ± SD (n = 6 chloroplasts per genotype), $^{**}p < 0.01$.

chorismate synthase downregulation in petunia, which increased many amino acids without changing aromatic amino acid levels (Zhong et al., 2020), the elevated leucine content does not necessarily mean that *NtIPMDs* are not involved in leucine biosynthesis, as leucine content may not directly reflect IPMD activity in planta. The strong valine accumulation may be due to a shift of carbon toward valine and weaker inhibition of valine synthesis when leucine production is reduced, as leucine branches from the valine pathway (Varghese et al., 2025; Engelgau and Beaudry, 2026). However, this possibility remains to be tested. AtIPMD has been reported to interact with LeuC (also named as IPDS) to form a complex involved in methionine chain-elongation and leucine biosynthesis (Chen et al., 2021). In contrast, our yeast two-hybrid assay did not detect an interaction between *NtIPMDs* and *NtIPDS* (data not shown). Together, these findings suggest that *NtIPMDs* may not be the main factor controlling leucine content in tobacco. Further studies, such as metabolic flux analysis and enzyme activity assays, will help clarify how *NtIPMDs* contribute to leucine and valine metabolism.

The reduced ABA and GA levels (Figure 7) may be associated with the chloroplast defects in *NtIPMD*-RNAi lines, although whether *NtIPMDs* directly regulate hormone biosynthesis remains

10.3389/fpls.2026.1979213

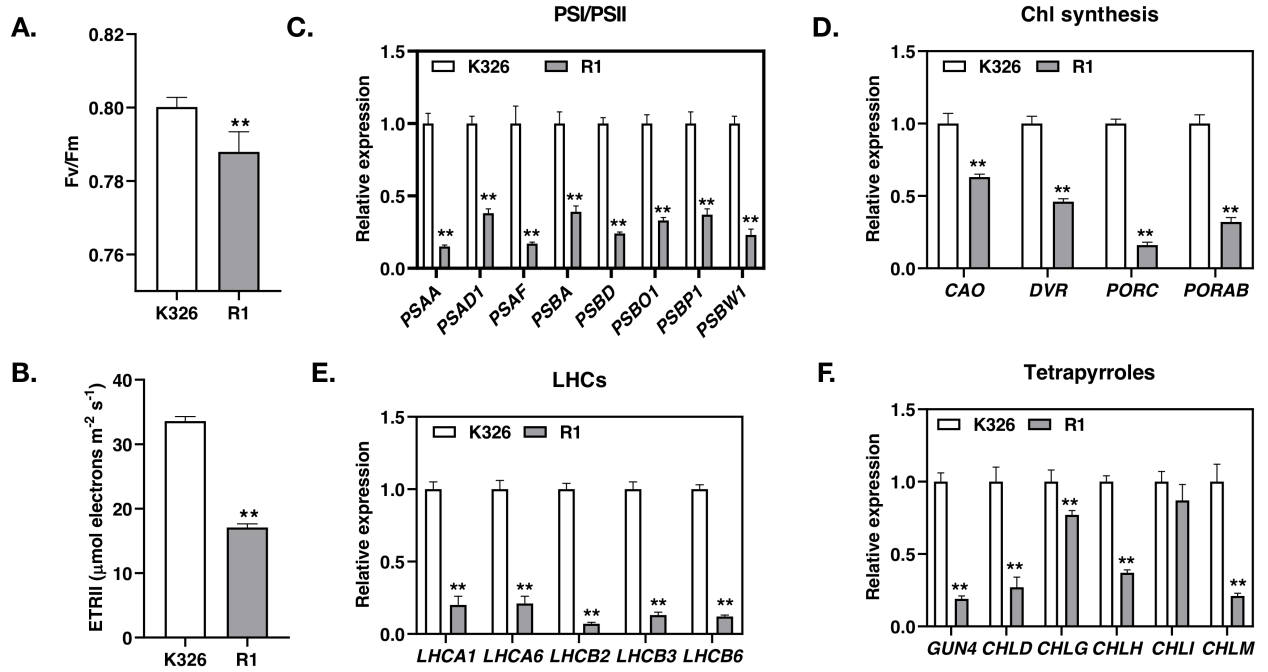


FIGURE 4
Photosynthetically related parameters and gene expression in *NtIPMD*-RNAi plants compared to K326. **(A)** Maximum quantum efficiency of PSII in the dark-adapted state (Fv/Fm) in R1 and K326. **(B)** The electron transport rate (ESRII) of R1 and K326. **(C–F)** Relative expression analysis of photosynthetic and chloroplast-related genes. Unpaired two-tailed Student's *t*-test was performed to compare *NtIPMD*-RNAi lines with the wild type. $^{**}p < 0.01$.

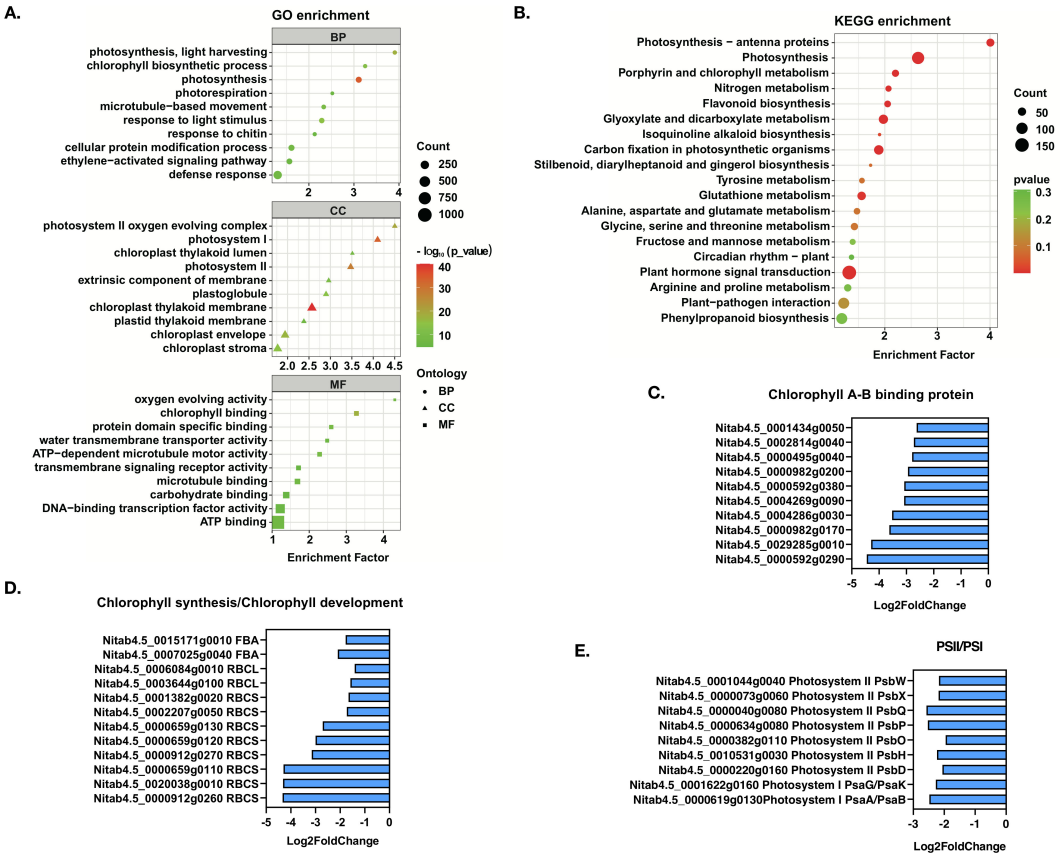


FIGURE 5
RNA-seq analysis of tobacco leaves in *NtIPMD*-RNAi lines and the wild type K326. **(A)** GO and **(B)** KEGG pathway enrichment analysis of the DEGs. **(C–E)** Different genes related to Chlorophyll a-b binding protein, chlorophyll synthesis/chlorophyll development, and PSII/PSI in RNA-seq.

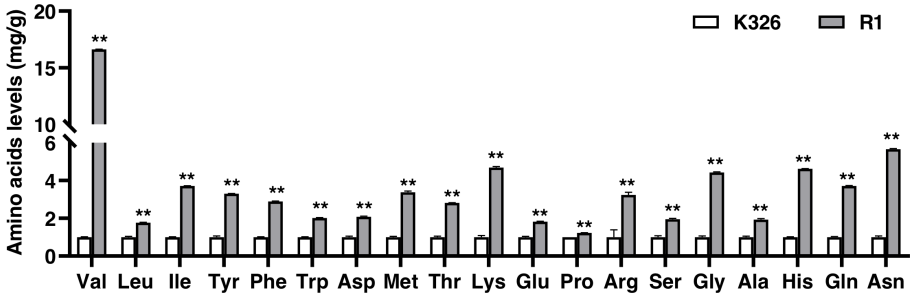


FIGURE 6
Amino acids contents in *NtIPMD*-RNAi plants and wild type K326. Unpaired two-tailed Student's *t*-test was performed to compare *NtIPMD*-RNAi lines with the wild type. $^{**}p < 0.01$.

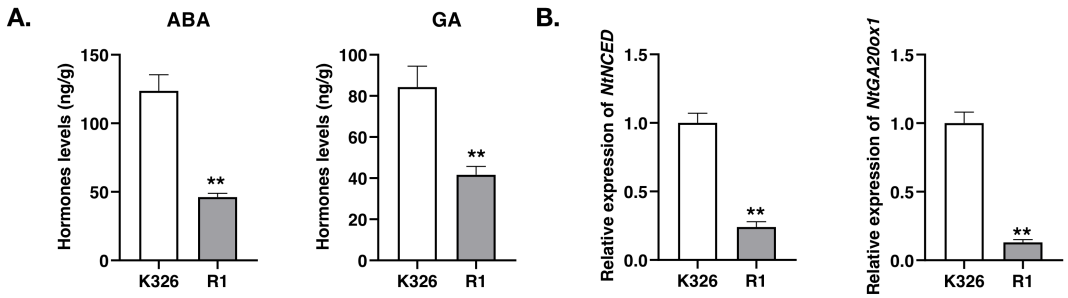


FIGURE 7
Hormone levels and the expression of related genes. **(A)** The contents of ABA and GA in *NtIPMD*-RNAi lines compared to K326. **(B)** Relative expression of *NtNCED* and *NtGA20ox1*. Unpaired two-tailed Student's *t*-test was performed to compare *NtIPMD*-RNAi lines with the wild type. $^{**}p < 0.01$.

unclear. These hormonal changes are more likely secondary consequences of the metabolic imbalance caused by *NtIPMD* silencing. Given that ABA positively regulates chloroplast ultrastructure and photosynthetic capacity, while GA promotes chloroplast division and thylakoid stacking (Cackett et al., 2022; Altamura et al., 2024), their reduction may further impair chloroplast development in these lines. Interestingly, a similar coordination of reduced ABA and GA levels has been observed in other plants with chloroplast development defects (Chao et al., 2014), suggesting a common stress response or developmental feedback mechanism. Whether *NtIPMDs* directly or indirectly affect hormone biosynthesis remains an open question. One possibility is that the dramatic accumulation of valine or other branched-chain amino acids may disturb hormone metabolic pathways. For instance, silencing of *NtBCAT* in *N. benthamiana* altered gibberellin and cytokinin levels (Gao et al., 2009), and exogenous valine application was shown to reduce gibberellin content in peach (Li et al., 2020), supporting the notion of crosstalk between BCAA metabolism and hormone signaling (Zhang et al., 2026). Further studies are needed to dissect the causal relationship between *NtIPMDs*, BCAA homeostasis, and phytohormone regulation.

The integrated transcriptomic and metabolomic analyses provide a multi-dimensional view of the consequences of *NtIPMDs* silencing. RNA-seq revealed widespread downregulation of photosynthesis-related genes, while metabolomics showed accumulation of most amino acids, particularly valine. Notably, GO enrichment analysis did not identify strongly enriched amino acid metabolism terms, except for a weak signal for cellular amino acid catabolic process (GO:0009063, adjusted $p = 0.04$). KEGG analysis showed enrichment of several amino acid metabolism pathways, including "alanine, aspartate and glutamate metabolism", "glycine, serine and threonine metabolism", "arginine and proline metabolism", "tyrosine metabolism", and "glutathione metabolism". These results suggest that the increased amino acid levels are not primarily driven by transcriptional upregulation of amino acid biosynthetic genes. Instead, they may result from post-transcriptional or metabolic-level changes, such as altered protein turnover or feedback regulation. The downregulation of hormone biosynthesis genes (*NtNCED*, *NtGA20ox1*) further supports the notion that NtIPMDs play a broader regulatory role beyond their canonical enzymatic function. Future studies employing targeted metabolomics, enzyme activity assays, and metabolic flux analysis will help elucidate the precise mechanisms by which NtIPMDs influence chloroplast development, amino acid homeostasis, and hormone signaling in tobacco.

Conclusion

In summary, this study characterized two chloroplast-localized isopropylmalate dehydrogenases (NtIPMDs) in tobacco. Silencing of *NtIPMDs* was associated with impaired chloroplast development

and altered metabolism, including changes in amino acid and hormones. However, whether these effects are direct or indirect remains to be determined. Our findings provide a basis for future studies on the functional diversity of *IPMD* genes in plants.

Data availability statement

The raw data sets analyzed during this study are available on NCBI under accession: PRJNA1330539.

Author contributions

NZ: Investigation, Writing – review & editing. PZ: Investigation, Writing – review & editing. YL: Validation, Writing – review & editing. HnZ: Conceptualization, Writing – review & editing. GX: Validation, Writing – review & editing. ZL: Formal analysis, Writing – review & editing. PL: Formal analysis, Writing – review & editing. LJ: Validation, Writing – review & editing. ZQ: Data curation, Writing – review & editing. HZ: Conceptualization, Data curation, Formal analysis, Funding acquisition, Investigation, Validation, Writing – original draft, Writing – review & editing.

Funding

The author(s) declared that financial support was received for this work and/or its publication. This work was supported by the National Natural Science Foundation of China (Grant No. 32000263) and the chief scientist innovation project of State Tobacco Monopoly Administration/China National Tobacco Corporation (932024CK0430).

Conflict of interest

The authors declare that this study received funding from State Tobacco Monopoly Administration/China National Tobacco Corporation. The funder was not involved in the study design, collection, analysis, interpretation of data, the writing of this article, or the decision to submit it for publication.

Generative AI statement

The author(s) declared that Generative AI was not used in the creation of this manuscript.

Any alternative text (alt text) provided alongside figures in this article has been generated by Frontiers with the support of artificial intelligence and reasonable efforts have been made to ensure accuracy, including review by the authors wherever possible. If you identify any issues, please contact us.

Publisher's note

All claims expressed in this article are solely those of the authors and do not necessarily represent those of their affiliated organizations, or those of the publisher, the editors and the reviewers. Any product that may be evaluated in this article, or claim that may be made by its manufacturer, is not guaranteed or endorsed by the publisher.

Supplementary material

The Supplementary Material for this article can be found online at: https://www.frontiersin.org/articles/10.3389/fpls.2026.1979213/full#supplementary-material

SUPPLEMENTARY TABLE 1
Sequences of qPCR primers. *L25* and *26S* were used as internal reference genes. *NtIPMDs* primers amplify a conserved region shared by *NtIPMD1* and *NtIPMD2*.

SUPPLEMENTARY TABLE 2
Sequences of primers for subcellular localization.

SUPPLEMENTARY FIGURE 1
Alignment of NtIPMD and AtIPMD proteins.

SUPPLEMENTARY FIGURE 2
Construction of the pBWA(V)HS-NtIPMDs RNAi vector. **(A)** Schematic diagram of the RNAi construct. **(B)** Region of the intron-spliced hairpin RNA sequence used for RNA interference, targeting a conserved region shared by NtIPMD1 and NtIPMD2.

SUPPLEMENTARY FIGURE 3
Virus-induced gene silencing of *NtIPMDs*. **(A)** Phenotype of *NtIPMDs* VIGS plants. **(B)** Relative expression of *NtIPMDs* transcripts. Data represent the combined expression of *NtIPMD1* and *NtIPMD2* for the primers amplify a conserved region shared by both genes.

References

Ali, M. S., Kim, K. W., Dhakal, R., Choi, D., and Baek, K. H. (2015). Accumulation of high contents of free amino acids in the leaves of Nicotiana benthamiana by the co-suppression of NbClpC1 and NbClpC2 genes. *Plant Cell Rep.* 34, 355–365. doi: 10.1007/s00299-014-1714-4

Altamura, M. M., Piacentini, D., Della Rovere, F., Fattorini, L., Valletta, A., and Falasca, G. (2024). Plastid dynamism integrates development and environment. *Plant Physiol. Biochem.* 213, 108813. doi: 10.1016/j.plaphy.2024.108813

Baek, E., Yoon, J. Y., and Palukaitis, P. (2017). Validation of reference genes for quantifying changes in gene expression in virus-infected tobacco. *Virology* 510, 29–39. doi: 10.1016/j.virol.2017.06.029

Binder, S. (2010). Branched-chain amino acid metabolism in Arabidopsis thaliana. *Arabidopsis Book* 8, e0137. doi: 10.1199/tab.0137

Brown, J., Pirrung, M., and McCue, L. A. (2017). FQC Dashboard: integrates FastQC results into a web-based, interactive, and extensible FASTQ quality control tool. *Bioinformatics* 33, 3137–3139. doi: 10.1093/bioinformatics/btx373

Cackett, L., Luginbuehl, L. H., Schreier, T. B., Lopez-Juez, E., and Hibberd, J. M. (2022). Chloroplast development in green plant tissues: the interplay between light, hormone, and transcriptional regulation. *New Phytol.* 233, 2000–2016. doi: 10.1111/nph.17839

Chang, J., Zhang, F., Qin, H., Liu, P., Wang, J., and Wu, S. (2021). Mutation of SlARC6 leads to tissue-specific defects in chloroplast development in tomato. *Hortic. Res.* 8, 127. doi: 10.1038/s41438-021-00567-2

Chao, Y., Kang, J., Zhang, T., Yang, Q., Gruber, M. Y., and Sun, Y. (2014). Disruption of the homogentisate solanesyltransferase gene results in albino and dwarf phenotypes and root, trichome and stomata defects in Arabidopsis thaliana. *PloS One* 9, e94031. doi: 10.1371/journal.pone.0094031

Chen, L. Q., Chhajed, S., Zhang, T., Collins, J. M., Pang, Q., Song, W., et al. (2021). Protein complex formation in methionine chain-elongation and leucine biosynthesis. *Sci. Rep.* 11, 3524. doi: 10.1038/s41598-021-82790-4

Chuang, C. F., and Meyerowitz, E. M. (2000). Specific and heritable genetic interference by double-stranded RNA in Arabidopsis thaliana. *Proc. Natl. Acad. Sci. U.S.A.* 97, 4985–4990. doi: 10.1073/pnas.060034297

Dellero, Y., Heuillet, M., Marnet, N., Bellvert, F., Millard, P., and Bouchereau, A. (2020). Sink/source balance of leaves influences amino acid pools and their associated metabolic fluxes in winter oilseed rape (Brassica napus L.). *Metabolites* 10:150. doi: 10.3390/metabo10040150

Edwards, K. D., Fernandez-Pozo, N., Drake-Stowe, K., Humphry, M., Evans, A. D., Bombarely, A., et al. (2017). A reference genome for Nicotiana tabacum enables map-based cloning of homeologous loci implicated in nitrogen utilization efficiency. *BMC Genomics* 18, 448. doi: 10.1186/s12864-017-3791-6

Ellerstrom, M., Josefsson, L. G., Rask, L., and Ronne, H. (1992). Cloning of a cDNA for rape chloroplast 3-isopropylmalate dehydrogenase by genetic complementation in yeast. *Plant Mol. Biol.* 18, 557–566. doi: 10.1007/BF00040671

Engelgau, P., and Beaudry, R. M. (2026). Banana aroma is a result of acetohydroxyacid synthase and isopropylmalate synthase alternative isoforms that bypass feedback inhibition. *Proc. Natl. Acad. Sci. U.S.A.* 123, e2515301123. doi: 10.1073/pnas.2515301123

Fujita, M., Tamegai, H., Eguchi, T., and Kakinuma, K. (2001). Novel substrate specificity of designer 3-isopropylmalate dehydrogenase derived from Thermus thermophilus HB8. *Biosci. Biotechnol. Biochem.* 65, 2695–2700. doi: 10.1271/bbb.65.2695

Fumagalli, M., Vieira, F. G., Linderoth, T., and Nielsen, R. (2014). ngsTools: methods for population genetics analyses from next-generation sequencing data. *Bioinformatics* 30, 1486–1487. doi: 10.1093/bioinformatics/btu041

Gao, F., Wang, C., Wei, C., and Li, Y. (2009). A branched-chain aminotransferase may regulate hormone levels by affecting KNOX genes in plants. *Planta* 230, 611–623. doi: 10.1007/s00425-009-0973-8

Ghosh, S., and Chan, C. K. (2016). Analysis of RNA-Seq data using TopHat and Cufflinks. *Methods Mol. Biol.* 1374, 339–361. doi: 10.1007/978-1-4939-3167-5_18

Gouveia, D. G., Barrios, W. E. B., Martins, A. O., Cavalcanti, J. H., Rosado-Souza, L., Siqueira, J. A., et al. (2026). Lysine biosynthesis defines a metabolic checkpoint for gibberellin-mediated growth in Arabidopsis thaliana. *Plant Cell Environ.* 49, 5343–5357. doi: 10.1111/pce.70525

Graczer, E., Szimler, T., Garamszegi, A., Konarev, P. V., Labas, A., Olah, J., et al. (2016). Dual role of the active site residues of Thermus thermophilus 3-isopropylmalate dehydrogenase: chemical catalysis and domain closure. *Biochemistry* 55, 560–574. doi: 10.1021/acs.biochem.5b00839

He, Y., Chen, B., Pang, Q., Strul, J. M., and Chen, S. (2010). Functional specification of Arabidopsis isopropylmalate isomerases in glucosinolate and leucine biosynthesis. *Plant Cell Physiol.* 51, 1480–1487. doi: 10.1093/pcp/pcq113

He, Y., Chen, L., Zhou, Y., Mawhinney, T. P., Chen, B., Kang, B. H., et al. (2011a). Functional characterization of Arabidopsis thaliana isopropylmalate dehydrogenases reveals their important roles in gametophyte development. *New Phytol.* 189, 160–175. doi: 10.1111/j.1469-8137.2010.03460.x

He, Y., Galant, A., Pang, Q., Strul, J. M., Balogun, S. F., Jez, J. M., et al. (2011b). Structural and functional evolution of isopropylmalate dehydrogenases in the leucine and glucosinolate pathways of Arabidopsis thaliana. *J. Biol. Chem.* 286, 28794–28801. doi: 10.1074/jbc.M111.262519

He, Y., Mawhinney, T. P., Preuss, M. L., Schroeder, A. C., Chen, B., Abraham, L., et al. (2009). A redox-active isopropylmalate dehydrogenase functions in the biosynthesis of glucosinolates and leucine in Arabidopsis. *Plant J.* 60, 679–690. doi: 10.1111/j.1365-313X.2009.03990.x

Hess, W. R., and Borner, T. (1999). Organellar RNA polymerases of higher plants. *Int. Rev. Cytol.* 190, 1–59. doi: 10.1016/s0074-7696(08)62145-2

Jackson, S. D., Sonnewald, U., and Willmitzer, L. (1993). Cloning and expression analysis of beta-isopropylmalate dehydrogenase from potato. *Mol. Gen. Genet.* 236, 309–314. doi: 10.1007/BF00277127

Kim, D., Paggi, J. M., Park, C., Bennett, C., and Salzberg, S. L. (2019). Graph-based genome alignment and genotyping with HISAT2 and HISAT-genotype. *Nat. Biotechnol.* 37, 907–915. doi: 10.1038/s41587-019-0201-4

Kowalewska, L., Mazur, R., Suski, S., Garstka, M., and Mostowska, A. (2016). Three-dimensional visualization of the tubular-lamellar transformation of the internal plastid membrane network during runner bean chloroplast biogenesis. *Plant Cell* 28, 875–891. doi: 10.1105/tpc.15.01053

Lee, S. G., Nwumeh, R., and Jez, J. M. (2016). Structure and mechanism of isopropylmalate dehydrogenase from Arabidopsis thaliana: insights on leucine and aliphatic glucosinolate biosynthesis. *J. Biol. Chem.* 291, 13421–13430. doi: 10.1074/jbc.M116.730358

Li, J. Y., Yang, C., Tian, Y. Y., and Liu, J. X. (2022). Regulation of chloroplast development and function at adverse temperatures in plants. *Plant Cell Physiol.* 63, 580–591. doi: 10.1093/pcp/pcac022

Li, S., Peng, F., Xiao, Y., Gong, Q., Bao, Z., Li, Y., et al. (2020). Mechanisms of high concentration valine-mediated inhibition of peach tree shoot growth. *Front. Plant Sci.* 11, 603067. doi: 10.3389/fpls.2020.603067

Li, Z., Zhou, H., Xu, G., Zhang, P., Zhai, N., Zheng, Q., et al. (2023). Genome-wide analysis of long noncoding RNAs in response to salt stress in Nicotiana tabacum. *BMC Plant Biol.* 23, 646. doi: 10.1186/s12870-023-04659-0

Liebers, M., Cozzi, C., Uecker, F., Chambon, L., Blanvillain, R., and Pfannschmidt, T. (2022). Biogenic signals from plastids and their role in chloroplast development. *J. Exp. Bot.* 73, 7105–7125. doi: 10.1093/jxb/erac344

Liu, X., Yu, F., and Rodermel, S. (2010). Arabidopsis chloroplast FtsH, var2 and suppressors of var2 leaf variegation: a review. *J. Integr. Plant Biol.* 52, 750–761. doi: 10.1111/j.1744-7909.2010.00980.x

Love, M. I., Huber, W., and Anders, S. (2014). Moderated estimation of fold change and dispersion for RNA-seq data with DESeq2. *Genome Biol.* 15, 550. doi: 10.1186/s13059-014-0550-8

Miggiano, R., Martignon, S., Minassi, A., Rossi, F., and Rizzi, M. (2020). Crystal structure of Haemophilus influenzae 3-isopropylmalate dehydrogenase (LeuB) in complex with the inhibitor O-isobutenyl oxalylhydroxamate. *Biochem. Biophys. Res. Commun.* 524, 996–1002. doi: 10.1016/j.bbrc.2020.02.022

Nozawa, A., Takano, J., Miwa, K., Nakagawa, Y., and Fujiwara, T. (2005). Cloning of cDNAs encoding isopropylmalate dehydrogenase from Arabidopsis thaliana and accumulation patterns of their transcripts. *Biosci. Biotechnol. Biochem.* 69, 806–810. doi: 10.1271/bbb.69.806

Pallo, A., Olah, J., Graczer, E., Merli, A., Zavodszky, P., Weiss, M. S., et al. (2014). Structural and energetic basis of isopropylmalate dehydrogenase enzyme catalysis. *FEBS J.* 281, 5063–5076. doi: 10.1111/febs.13044

Rui, L., Yang, S. Q., Zhou, X. H., and Wang, W. (2025). The important role of chloroplasts in plant immunity. *Plant Commun.* 6, 101420. doi: 10.1016/j.xplc.2025.101420

Scotti, N., and Tamburino, R. (2026). Chloroplasts and plant sustainability: key roles and emerging insights. *Int. J. Mol. Sci.* 27:4675. doi: 10.3390/ijms27114675

Siddik, M. A. B., and Shin, A. C. (2019). Recent progress on branched-chain amino acids in obesity, diabetes, and beyond. *Endocrinol. Metab. (Seoul)* 34, 234–246. doi: 10.3803/EnM.2019.34.3.234

Slocombe, S. P., Schauvinhold, I., McQuinn, R. P., Besser, K., Welsby, N. A., Harper, A., et al. (2008). Transcriptomic and reverse genetic analyses of branched-chain fatty acid and acyl sugar production in Solanum pennellii and Nicotiana benthamiana. *Plant Physiol.* 148, 1830–1846. doi: 10.1104/pp.108.129510

Svab, Z., and Maliga, P. (1993). High-frequency plastid transformation in tobacco by selection for a chimeric aadA gene. *Proc. Natl. Acad. Sci. U.S.A.* 90, 913–917. doi: 10.1073/pnas.90.3.913

Varghese, M., Kumar, R., Sharma, A., Lone, A., Gershenzon, J., and Bisht, N. C. (2025). Isopropylmalate synthase regulatory domain removal abolishes feedback regulation at the expense of leucine homeostasis in plants. *Plant Physiol.* 197:kiaf041. doi: 10.1093/plphys/kiaf041

Wang, J., Zhang, Q., Tung, J., Zhang, X., Liu, D., Deng, Y., et al. (2024). High-quality assembled and annotated genomes of Nicotiana tabacum and Nicotiana benthamiana reveal chromosome evolution and changes in defense arsenals. *Mol. Plant* 17, 423–437. doi: 10.1016/j.molp.2024.01.008

Wang, X., Li, Q., Zhang, Y., Pan, M., Wang, R., Sun, Y., et al. (2022). VAR2/AtFtsH2 and EVR2/BCM1/CBD1 synergistically regulate the accumulation of PSII reaction centre D1 protein during de-etiolation in Arabidopsis. *Plant Cell Environ.* 45, 2395–2409. doi: 10.1111/pce.14368

Waters, M. T., and Langdale, J. A. (2009). The making of a chloroplast. *EMBO J.* 28, 2861–2873. doi: 10.1038/emboj.2009.264

Xie, J., Chen, Y., Cai, G., Cai, R., Hu, Z., and Wang, H. (2023). Tree visualization by one table (tvBOT): a web application for visualizing, modifying and annotating phylogenetic trees. *Nucleic Acids Res.* 51, W587–W592. doi: 10.1093/nar/gkad359

Yu, G., Wang, L. G., Han, Y., and He, Q. Y. (2012). clusterProfiler: an R package for comparing biological themes among gene clusters. *OMICS* 16, 284–287. doi: 10.1089/omi.2011.0118

Zhang, H., Li, Z., Xu, G., Bai, G., Zhang, P., Zhai, N., et al. (2022). Genome-wide identification and characterization of NPF family reveals NtNPF6.13 involving in salt stress in Nicotiana tabacum. *Front. Plant Sci.* 13, 999403. doi: 10.3389/fpls.2022.999403

Zhang, Y., Tian, L., and Lu, C. (2023). Chloroplast gene expression: Recent advances and perspectives. *Plant Commun.* 4, 100611. doi: 10.1016/j.xplc.2023.100611

Zhang, H., Zheng, Q., Xu, G., Zhai, N., Li, Z., Zhang, P., et al. (2024). Involvement of isopropylmalate dehydratase in chloroplast development and acylsugar accumulation in tobacco. *Ind. Crops Prod.* 222, 119543. doi: 10.1016/j.indcrop.2024.119543

Zhang, X., Zhou, Y., Shamsi, I. H., Jiang, L., Wang, S., Zhao, Y., et al. (2026). Paraburkholderia sp. GD17 alleviates damage under drought stress by inducing abscisic acid to regulate the branched-chain amino acid pathway. *Plant Physiol. Biochem.* 233, 111260. doi: 10.1016/j.plaphy.2026.111260

Zheng, M., Liu, X., Liang, S., Fu, S., Qi, Y., Zhao, J., et al. (2016). Chloroplast translation initiation factors regulate leaf variegation and development. *Plant Physiol.* 172, 1117–1130. doi: 10.1104/pp.15.02040

Zhong, S., Chen, Z., Han, J., Zhao, H., Liu, J., and Yu, Y. (2020). Suppression of chorismate synthase, which is localized in chloroplasts and peroxisomes, results in abnormal flower development and anthocyanin reduction in petunia. *Sci. Rep.* 10, 10846. doi: 10.1038/s41598-020-67671-6